Wind observations of foreshock cavities: A case study

D. G. Sibeck[1]
Applied Physics Laboratory, Johns Hopkins University, Laurel, Maryland, USA

T.-D. Phan and R. Lin
Space Sciences Laboratory, University of California, Berkeley, California, USA

R. P. Lepping and A. Szabo
Goddard Space Flight Center, Greenbelt, Maryland, USA

Received 6 July 2001; revised 7 January 2002; accepted 22 April 2002; published 4 October 2002.

[1] We present a case study of plasma, energetic particle, and magnetic field perturbations seen by Wind in the dawn foreshock on 19 April 1996. A comparison with the results of hybrid simulations confirms model predictions for a diamagnetic cavity flanked by regions of enhanced density and magnetic field strength but filled with a suprathermal ion population. In contrast to previously reported hot flow anomalies, flow velocities within the foreshock cavities are nearly identical to those in the ambient solar wind, ion temperatures do not rise greatly, thermal pressures are only slightly greater than those in the ambient solar wind, and the events do not lie centered upon interplanetary magnetic field (IMF) tangential discontinuities intersecting the bow shock. We attribute the cavities to the diamagnetic effects of ions Fermi accelerated within the foreshock. A review suggests that foreshock cavities are far more common than hot flow anomalies. *INDEX TERMS:* 2154 Interplanetary Physics: Planetary bow shocks; 2116 Interplanetary Physics: Energetic particles, planetary; 2784 Magnetospheric Physics: Solar wind/magnetosphere interactions; *KEYWORDS:* foreshock, bow shock, cavities, pulses, energetic ions

Citation: Sibeck, D. G., T.-D. Phan, R. Lin, R. P. Lepping, and A. Szabo, Wind observations of foreshock cavities: A case study, *J. Geophys. Res.*, *107*(A10), 1271, doi:10.1029/2001JA007539, 2002.

1. Introduction

[2] Kinetic processes within the foreshock can significantly modify the solar wind just prior to its interaction with the Earth's bow shock and magnetosphere. To simulate these processes within a magnetohydrodynamic (MHD) model, *Skadron et al.* [1986] simply introduced a 30 R_E wide band of enhanced pressures into the region upstream from a planar bow shock. The pressure diminished abruptly at the dawn and dusk edges of the band, but only gradually in the sunward direction. They predicted enhanced solar wind densities and magnetic field strengths just outside the dawn/dusk boundaries of the foreshock, diminished densities and magnetic field strengths just inside, and slightly enhanced solar wind densities and slightly diminished solar wind velocities deep within the foreshock. Flows at the dawn and dusk boundaries of the foreshock were deflected away from the Earth-Sun line. Although they obtained relatively minor perturbations ($\Delta V \sim 1.5\%$, $n = B \sim 7.5\%$, $_V \sim 1.5°$) for realistic foreshock pressures, *Skadron et al.* [1986] noted that the strength of the perturbations increased almost linearly with the intensity/pressure of the suprathermal ions.

[3] *Thomas and Brecht* [1988] presented a more self-consistent hybrid simulation for a similar problem. They launched a narrow (4000 km) beam of hot ($V_{th}/V_A = 2$), tenuous ($n_{beam}/n_{sw} = 0.1$), sunward streaming reflected ions into the superAlfvénic ($V_{sw}/V_A = 10$), cold ($V_{th} = 0$), solar wind flow along a band of field lines connected to the bow shock. The counterstreaming populations initiated electromagnetic ion instabilities that scattered the reflected ions to form a diffuse suprathermal population surrounding a decelerated solar wind flow. As the successive snapshots shown in Figure 1 illustrate, the solar wind distribution broadened and decelerated slightly. The beam of backstreaming ions was initially scattered primarily in the direction transverse to the magnetic field to form an intermediate (or kidney-shaped) distribution, and then thermalized almost completely to form a spherical halo (or diffuse population) around the antisunward moving solar wind distribution. By the end of the simulation, the distribution function for the combined particle populations was smooth with only a single peak.

[4] As indicated in Figure 2, the enhanced temperatures and pressures associated with the suprathermal ions created a crater-like diamagnetic cavity of depressed plasma densities and magnetic field strengths on the band of field lines

[1]Now at NASA Goddard Space Flight Center, Greenbelt, Maryland, USA.

0148-0227/02/2001JA007539$09.00

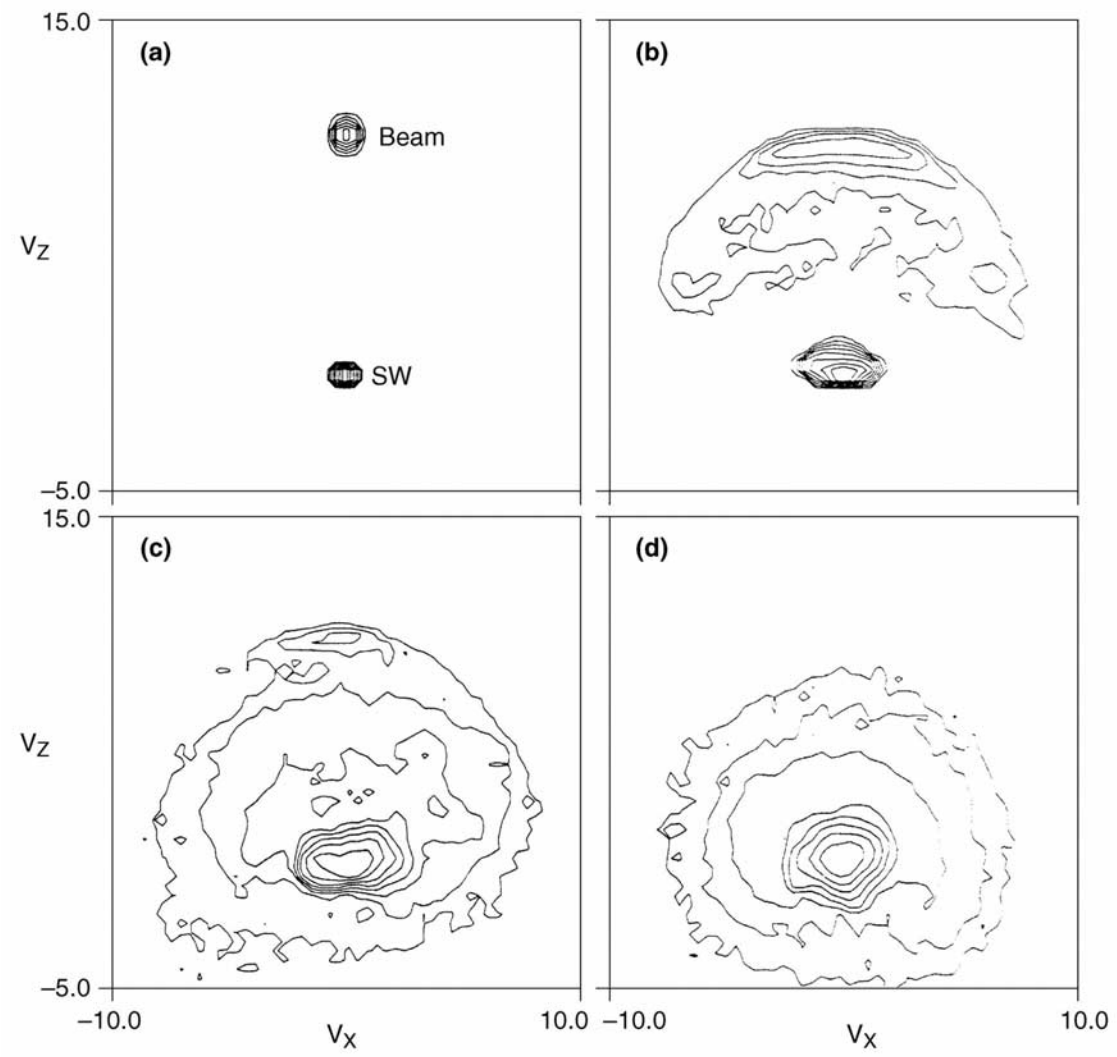

Figure 1. Thomas and Brecht model predictions for distribution functions within foreshock cavities at four times: (a) $\omega_{ci}t = 22$ (the initial appearance of the beams), (b) $\omega_{ci}t = 36$, (c) $\omega_{ci}t = 43$, and (d) $\omega_{ci}t = 50$. The scale is logarithmic with approximately 2 levels per decade, and ω_{ci} is the ion plasma frequency. A spatial average has been made over the initial width of the ion beam. The distribution functions are shown in the rest frame of the solar wind.

connected to the bow shock. The plasma and magnetic field excavated from the interior of the cavity piled up as density and magnetic field strength enhancements on the edges of the band, where field lines were not connected to the bow shock. The pile-up, corresponding to a fast mode compressional pulse, moved away from the beam. Perturbation amplitudes increased steadily with time. Less than a minute into the simulation, there were ~30–40% density and magnetic field strength decreases within the beam and ~50% increases on its edges.

[5] Events with the features predicted by the *Thomas and Brecht* [1988] model have been observed within the Earth's foreshock. *Thomsen et al.* [1986] reported that hot flow anomalies (HFAs) exhibit durations of 1–2 min, reduced densities and magnetic field strengths flanked on one or both sides by enhancements, strongly reduced flow speeds, nearly isotropic and Maxwellian distributions within the central cavity, and a gradual increase in temperatures from the solar wind into the cavity. They noted superposed hot and cold distributions on exit from one such cavity.

[6] HFAs also exhibit some features not predicted by the model of *Thomas and Brecht* [1988]. The events have primarily been identified on the basis of strong flows transverse to the Sun–Earth line [*Thomsen et al.*, 1986] and greatly diminished antisunward or even slightly sunward flows [*Paschmann et al.*, 1988]. The greatly diminished antisunward flows within the events require a strong shock on the trailing, sunward, edge. The presence of energetic (>70 keV) electrons in almost all HFAs suggests not only that they always occur on IMF lines that graze the magnetopause, but also that they occur on reconnected field lines [*Paschmann et al.*, 1988].

[7] *Onsager et al.* [1990] noted that temperatures ($T_e \sim 10^6$ K, $T_I \sim 10^7$ K) and pressures within HFAs far exceed those predicted for the adiabatic expansion of completely thermalized counterstreaming solar wind and reflected pop-

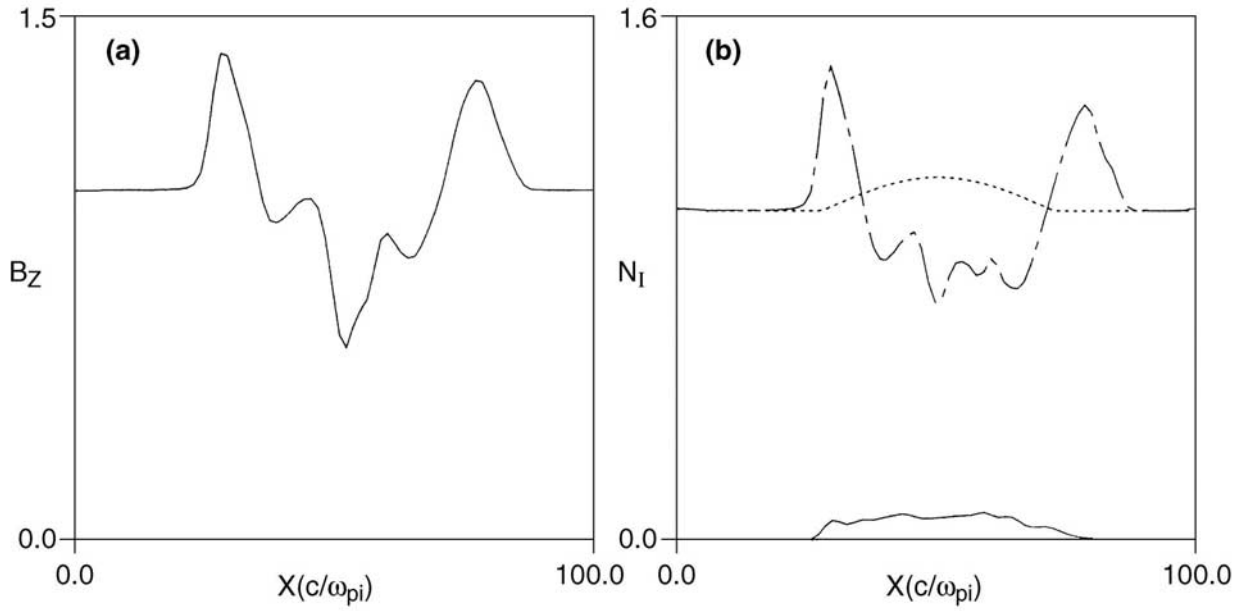

Figure 2. Thomas and Brecht model predictions for cavity cross sections at $\omega_{ci}t = 43$: (a) the magnetic field strength, and (b) the ion densities. The dashed line indicates values for the background ions, the solid line those for the beam ions, and the dotted line those for the initial ion density.

ulations to densities well below those of the ambient solar wind. As a result, *Thomas et al.* [1991] abandoned the *Thomas and Brecht* [1988] model in favor of one involving the interaction of a sharp interplanetary magnetic field (IMF) discontinuity with the bow shock. The ions are energized by electric fields pointing inward toward the discontinuity, scattered and thermalized by encounters with the bow shock, and confined to the vicinity of the discontinuity by trapped orbits that gyrate about the discontinuity. Global simulations subsequently confirmed that IMF discontinuities interacting with the bow shock can produce strong localized flow deflections [*Lin*, 1997], and a review of previously reported HFAs indicated that most, if not all, can be associated with abrupt IMF rotations [*Schwartz et al.*, 2000].

[8] The 3DP instrument on Wind provides solar wind plasma observations with full three-dimensional coverage at higher time resolution than was available in previous studies. We begin by presenting Wind 3DP plasma, energetic particle, and MFI magnetic field observations of two foreshock cavities whose internal structures greatly resemble those predicted by *Thomas and Brecht* [1988] model. We distinguish the two events from HFAs by showing that they exhibit no significant flow deflections, no association with abrupt IMF discontinuities, and only modest increases in ion temperature. In fact, solar wind ion temperatures actually fall within the cavities, although overall ion temperatures rise due to the addition of a suprathermal ion population. Finally, we argue that Fermi-accelerated ions provide sufficient pressure to generate the diamagnetic foreshock cavities.

2. Data Sets

[9] We obtain plasma moments and energetic particle phase space densities from the 3DP three-dimensional plasma and energetic particle detectors [*Lin et al.*, 1995] on the Wind spacecraft. The 3DP PESA-L "top-hat" electrostatic analyzer observes the core solar wind ions over an energy range covering an order of magnitude that is centered upon the time dependent mean solar wind energy (~1.15 to 11.6 keV). PESA-H detects suprathermal ions in the 80 eV-27 keV energy range. EESA-L measures electrons from 10 eV to 1.1 keV while EESA-H detects electrons with energies from 135 eV to 27 keV. Due to limited telemetry, PESA-H and EESA-H distributions are averaged on board over 51s before transmission. PESA-L and EESA-L transmit proton and electron moments for the core solar wind proton distributions each 3s spacecraft spin. Finally, two solid state semiconductor telescopes (SST) with geometric factors of 0.3 keV-cm^2-sr provide energetic electron ($26 < E_e < 519$ keV) and ion ($67 < E_I < 6800$ keV) distributions each 51s. The MFI magnetometer [*Lepping et al.*, 1995] on Wind observes the vector magnetic field at a rate of 10.9 samples/s, but for our analysis the magnetic field data are averaged to 3s time resolution.

3. Observations

[10] During the 30 min period from 2000 to 2030 UT on 19 April 1996, Wind was located well upstream from the equatorial dawn bow shock, near GSE (x, y, z) = (9.0, −28.0, 2.5) R_E. As shown in Figure 3, Wind observed two crater-like structures in the IMF strength and solar wind density: a pronounced event from 2011 to 2017 UT and a weaker event with shorter duration from 2026 to 2028 UT. Like HFAs, both events exhibited enhanced densities and magnetic field strengths bounding central regions with depressed densities and magnetic field strengths.

[11] As in the case of HFAs, densities and magnetic field strengths within the cavities were highly correlated. Figure 4

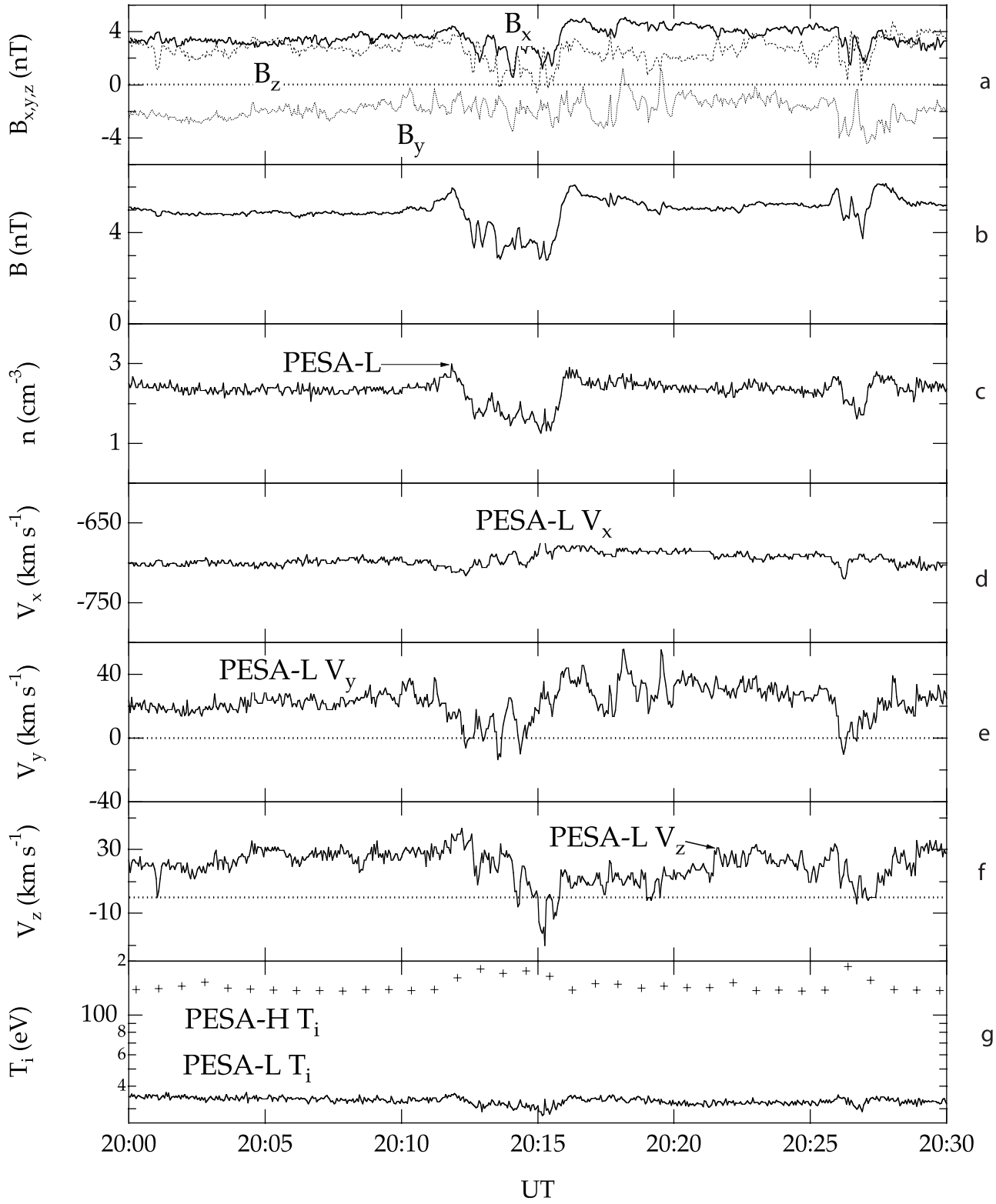

Figure 3. Wind 3DP plasma and MFI magnetic field observations from 2000 to 2030 UT on 19 April 1996. From top to bottom, the panels show (a) the three components of the magnetic field in GSE coordinates, (b) the total magnetic field strength, (c) core solar wind ion densities measured by PESA-L, (d–f) x, y, and z components of the solar wind flow velocity, (g) core solar wind (measured by PESA-L) and suprathermal (measured by PESA-H) total temperatures.

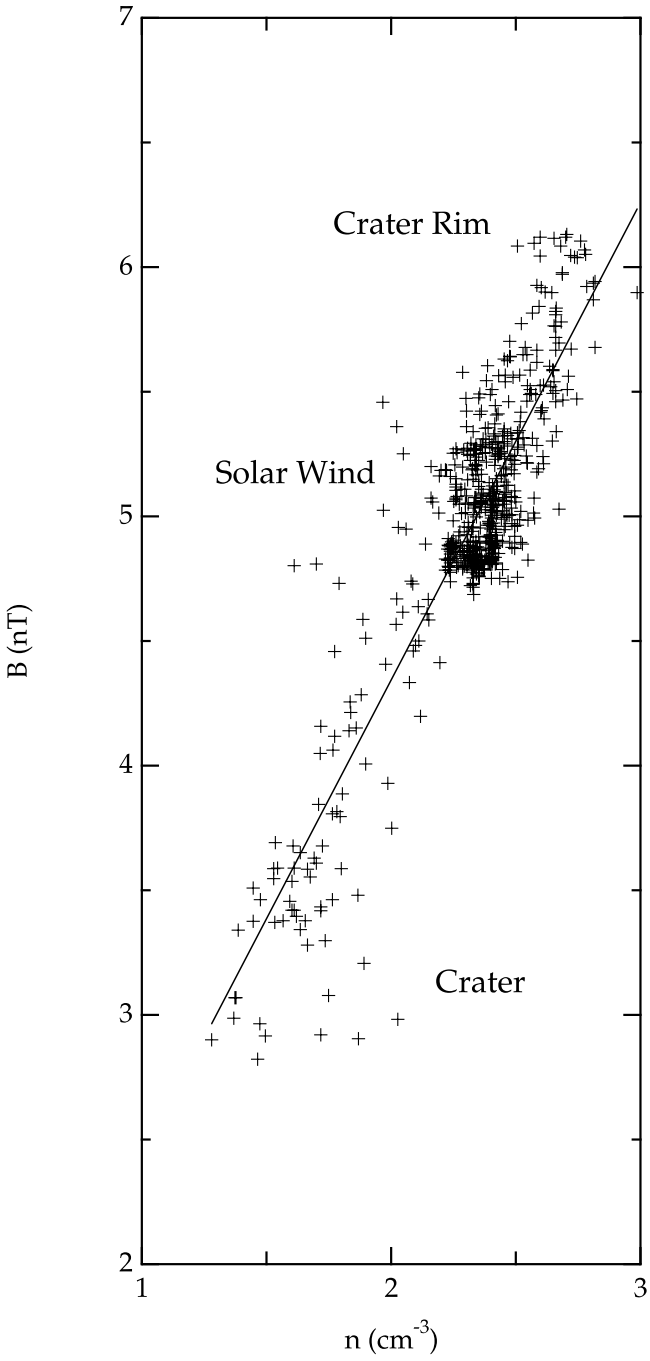

Figure 4. Wind MFI magnetic field strengths versus core solar wind densities (measured by PESA-L) for the interval from 2000 to 2030 UT on 19 April 1996.

presents a plot of the density versus the magnetic field strength for the entire 30 min interval. The two parameters were linearly correlated (B = 1.92 n + 0.51) with a correlation coefficient of 0.88. The large positive correlation coefficient indicates that most of the density and magnetic field strength variations seen during this interval can be interpreted in terms of fast mode waves.

[12] Other features of the events do not agree with past observations of HFAs. The magnitude of the flow velocity along the Sun-Earth line (V_X) diminished slightly from 700 to 680 km s^{-1} across the first event, and showed little variation across the second event. By contrast, the other two components of the solar wind velocity fell during both events. Consequently instead of being deflected far off the Sun-Earth line as is the case with HFAs, flow vectors within the core regions of these events were even more closely aligned with the Sun-Earth line.

[13] Rather than being associated with abrupt interplanetary magnetic field discontinuities marking the transition between two distinctly different IMF orientations (as in the case of HFAs), both events were simply associated with brief decreases in the (positive) B_z component of the IMF. As illustrated in Figure 5, these decreases allowed the otherwise sunward and dawnward IMF lines passing through Wind to graze the nominal location of the southern prenoon bow shock. Wave activity is enhanced in and near the cavities. This is most clearly seen in the ~30 s period variations of the B_y and V_y components that appear from 2010 to 2020 and 2025:30 to 2026:30 UT in Figure 3.

[14] Contrary to predictions from any of the numerical simulations, PESA-L observations indicated depressed solar wind ion temperatures within the central region of the events, but slightly enhanced temperatures on the crater rims. By contrast, PESA-H observations indicated greater ion temperatures within the central regions. The conflicting observations can be reconciled by invoking the presence of enhanced ion fluxes within the craters at energies greater than those that can be observed by PESA-L but which can be observed by PESA-H. If suprathermal ions are present, pressure considerations require the cavities to expand, and densities, core solar wind temperatures, and magnetic field strengths to fall.

[15] To confirm this hypothesis, we present phase space density traces in Figure 6. Whereas PESA-H recorded depressed ion fluxes at energies of 11.1 keV and below within the cavities, it recorded enhanced fluxes at energies of 17.4 keV and above. Because PESA-L only observed the former population, it recorded a temperature decrease within the cavities, rather than the temperature increase seen by PESA-H. A similar explanation probably accounts for the decrease in temperature seen by IMP-8 within a similar event [*Sibeck et al.*, 2001], as the MIT plasma detector on that spacecraft only measures ions with energies below 7 keV.

[16] The Wind 3DP SST observations shown in Figure 6 indicate that the energetic ion flux enhancements within the cavities extended to 333 keV. At higher energies, flux levels within the events were comparable to those in the ambient solar wind. The SST observations also indicate the presence of an energetic electron population extending from 27.2 to 108 keV and perhaps even to 182 keV during the first event. During the second event, the enhanced flux of electrons extended to energies no greater than 108 keV.

[17] Distribution functions within the foreshock cavities provide further opportunities for comparisons with the model predictions shown in Figure 1. Figure 7f presents a typical solar wind ion phase space distribution seen outside the cavities. The distribution peaks near $V_\perp = -V_\parallel \sim 500$ km s^{-1}, indicating a particle population carrying the sunward and dawnward pointing IMF antisunward. The phase space density of ions moving sunward falls to background levels at velocities greater than 1000 km s^{-1}. Note that

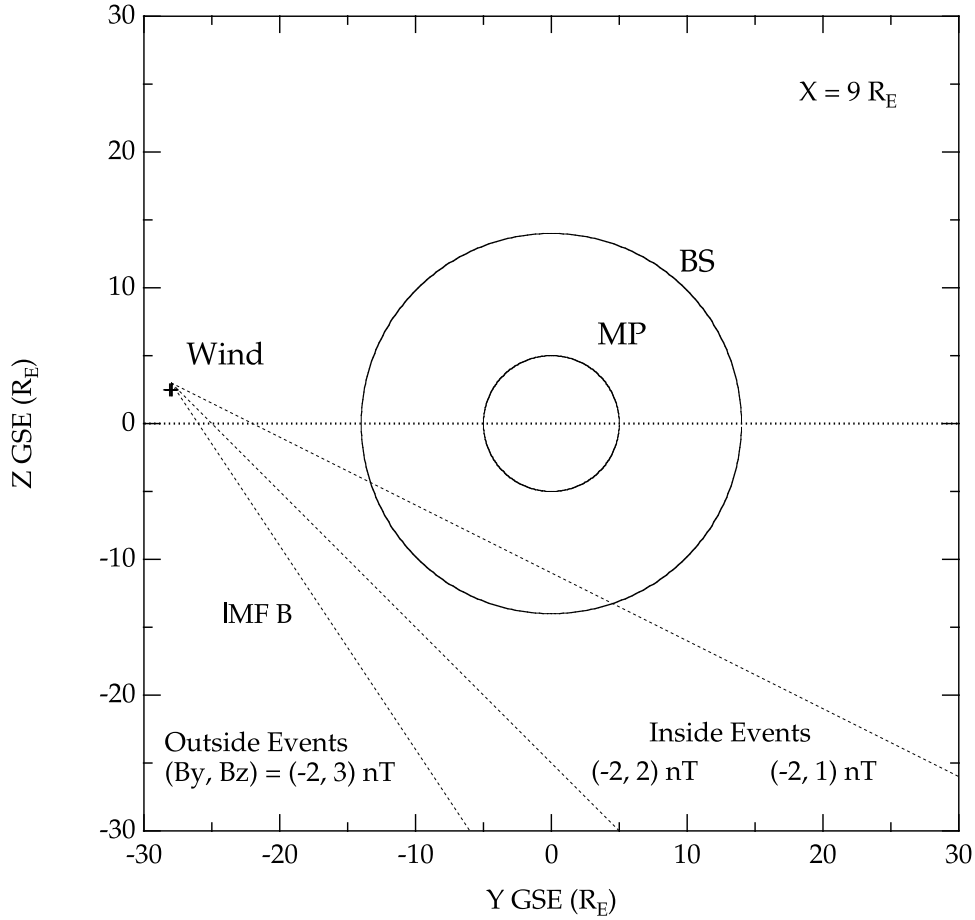

Figure 5. A cross section of the nominal [*Fairfield*, 1971] magnetopause and bow shock locations in the GSE Y-Z plane at X = 9 R_E. Dashed lines indicate the projection of selected IMF vectors observed both inside and outside the first Wind event into this plane. Crosses mark the location of Wind at 2030 UT.

observations near V = 0 have been deleted in this and other panels to obscure instrumental effects at low velocities. Figures 7a and 7e present phase space distributions taken on the rims of the craters. Both show additional ion beams with limited azimuthal extent moving sunward at velocities $V_{\parallel} \sim -V_{\perp} = 1200$ km s^{-1}. Figures 7b, 7c, and 7d, present phase space distributions within the core region of the cavity. Each shows the presence of suprathermal ions throughout a widespread azimuthal halo at velocities exceeding 2000 km s^{-1}.

[18] The sequence of phase space distributions seen in Figure 7 greatly resembles the model predictions shown in Figure 1. The distributions also typify those usually observed in the foreshock. Following the definitions of *Paschmann et al.* [1981], Figures 7a and 7e provide examples of reflected beams, whereas Figures 7b, 7c, and 7d provide examples of intermediate (semicircular) distributions tending towards isotropic or diffuse populations. By contrast, the distribution functions in Figure 7 differ strikingly from those seen during transitions through HFAs, where there is generally a gradual evolutionary increase in temperature rather than a mixing of hot and cold distributions [*Thomsen et al.*, 1986]. On those rare occasions when two populations have been observed within HFAs, they have taken either the form of a hot population flowing sunward superimposed upon a cold population with reduced densities flowing antisunward [*Thomsen et al.*, 1986], or reflected and incident solar wind beams with comparable densities merging to form heated core region plasmas [*Thomsen et al.*, 1988].

4. Discussion

[19] The discussion above noted the similarity of the foreshock cavity structure and ion distribution functions to those predicted by the model of *Thomas and Brecht* [1988], the fact that the IMF connected Wind to the bow shock during the events, and the presence of enhanced wave activity within and near the events. For all these reasons, we attribute the cavities to ion reflection from the bow shock, scattering and subsequent Fermi acceleration. In this section, we consider the origin of the energetic electrons seen within the cavities, the effects of the energetic particles upon the ambient solar wind plasma, and the boundaries of the events.

[20] A considerable body of work indicates that Fermi acceleration can easily supply ion spectra that extend to ~300 keV, as in the cases presented here. On the other

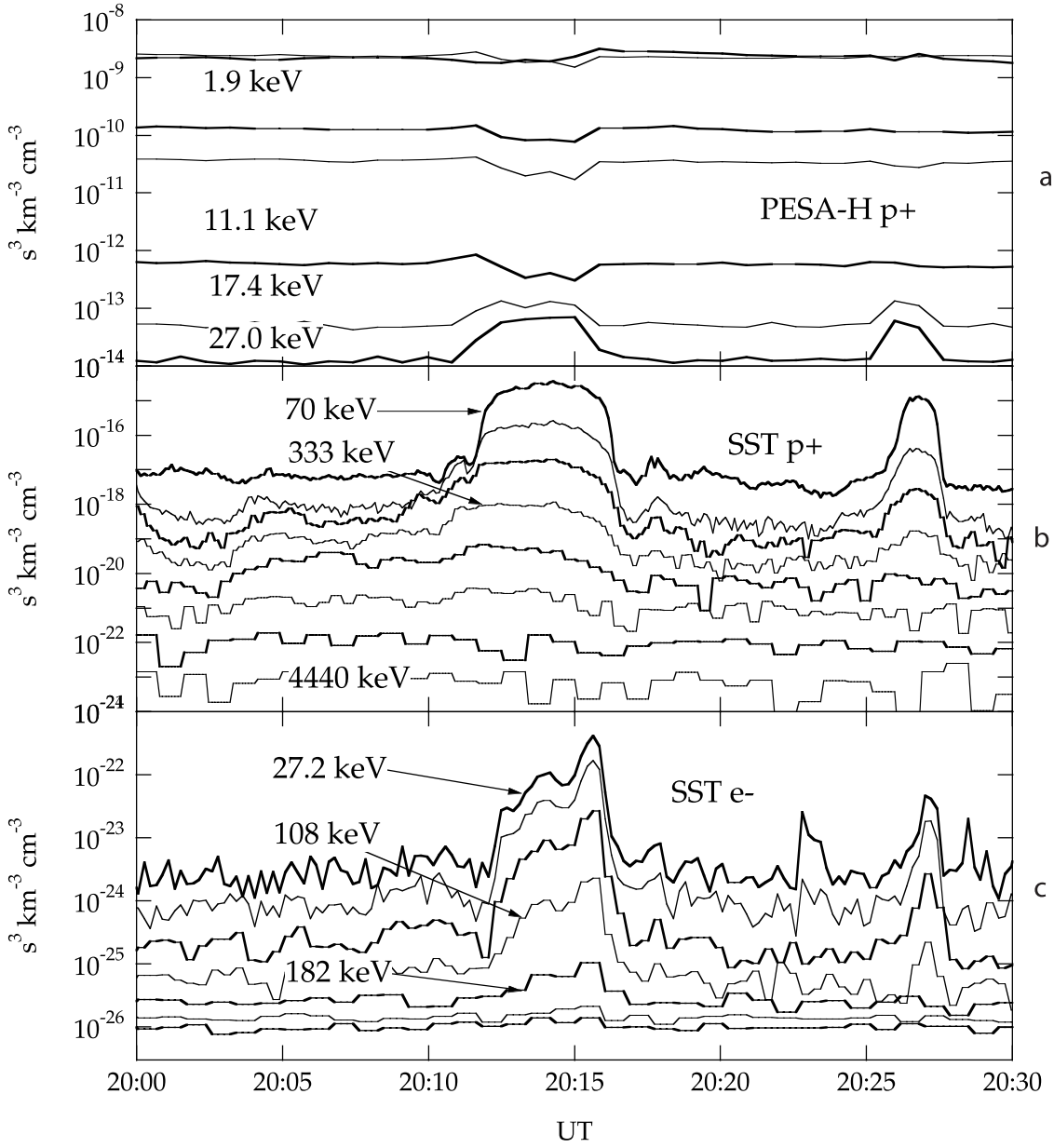

Figure 6. Wind 3DP phase space densities versus time. From top to bottom: (a) PESA-H ion observations from 1.9 to 27.0 keV, (b) SST ion observations from 70 to 4440 keV, (c) SST electron observations from 27.2 to 519 keV.

hand, *Scholer et al.* [1981] reported that energetic electrons are absent within such events. In principle, the energetic electrons (and some or all of the ions) seen within our cavities could have originated within the magnetosphere. However, this seems unlikely given the IMF orientation shown in Figure 5. While the IMF probably connected Wind to the southern dawn bow shock during the events, it certainly did not connect Wind to the magnetopause. Since the IMF only grazed the bow shock, fast Fermi or shock-drift acceleration provides a better explanation for the energetic electron population seen within the cavities. Past reports indicate that electrons with energies up to ~100 keV appear on magnetic field lines that graze the bow shock [e.g., *Anderson et al.*, 1979].

[21] Pressures associated with energetic ions in the foreshock can greatly perturb the incoming solar wind prior to its interaction with the bow shock and magnetosphere. *Mitchell and Roelof* [1983] have already noted that the energy density within Fermi-accelerated foreshock ion beams is comparable to that of the ambient magnetic field. *Sibeck et al.* [2001] showed that the energetic ion population can supply the pressures required to explain diamagnetic cavities within the foreshock. In our case, the low time resolution of the PESA-H ion temperatures precludes a direct calculation of the pressures inside the cavities. Nevertheless, we can estimate the pressure within the cavities by calculating the sum of the ion thermal and magnetic pressures in the rims under an assumption that rim temper-

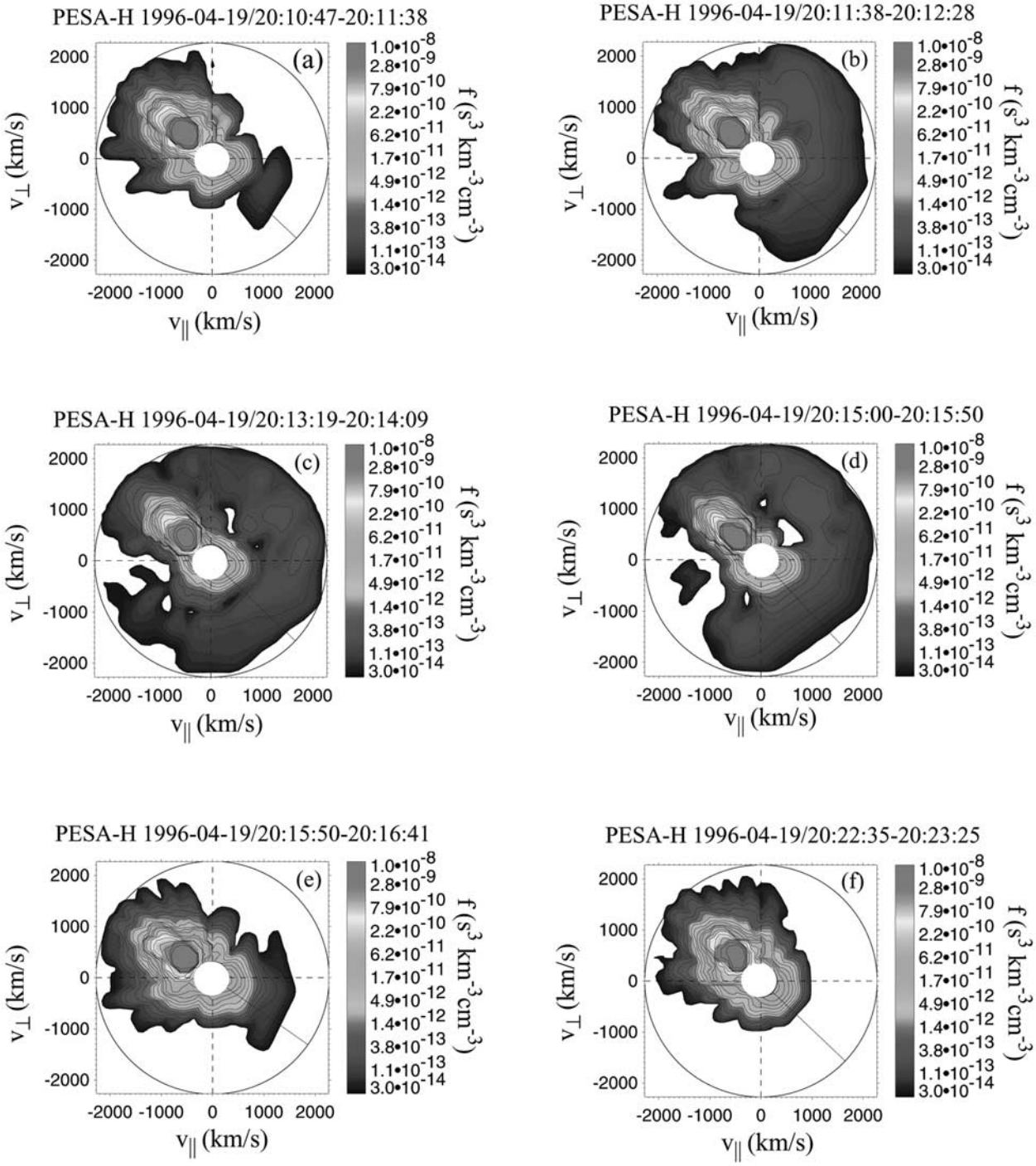

Figure 7. Wind 3DP PESA-H ion distribution functions from (a) 2010:47 to 2011:38, (b) 2011:38 to 2012:28, (c) 2013:19 to 2014:09, (d) 2015:00 to 2015:50, (e) 2015:50 to 2016:41, and (f) 2022:35 to 2023:25 UT. See color version of this figure at back of this issue.

atures are identical to those in the ambient solar wind. Since the temperature within the rims is presumably greater than that in the solar wind proper, and the pressure within the cavity greater than that in the rims, our calculation underestimates the pressure within the cavity. Even with these assumptions, we find that the sum of the pressures within the first cavity (~0.058 nPa) exceeds that in the ambient solar wind (0.048 nPa). The cavities should therefore grow with time.

[22] We next examine the hypothesis that the cavities grow with time via the ongoing introduction of suprathermal ions via Fermi acceleration in the foreshock, rather than collapsing following an initial explosion, as suggested by *Onsager et al.* [1990]. *Terasawa* [1979] has used the Fermi model to predict ion flux and spectra throughout the equatorial foreshock during a period of spiral IMF. His model results indicate that flux levels of 45 keV ions immediately outside the bow shock increase by a factor of

6.6 from 300 to 2000 $(cm^2\text{-s-ster-keV})^{-1}$ and the spectral index γ increases from 2 to 3.5 from 1.5 to 5 min following initial contact of the interplanetary magnetic field lines with the bow shock.

[23] As noted by *Sibeck et al.* [2001], the contribution to the pressure P within the energy range from T_1 to T_2 from a power law distribution of isotropic energetic ions is given by

$$P_{12} = (4\pi/3)(2mT_0)^{1/2}[\, j(T_0)T_0]\left[\frac{\tau_1^{-\gamma+3/2} - \tau_2^{-\gamma+3/2}}{\gamma - 3/2}\right] \quad (1)$$

where $j(T_0)$ is the intensity at reference energy T_0, m is the particle mass, assumed here to be that of a proton, and γ is the spectral index of the power law distribution. Using the aforementioned values provided by *Terasawa* [1979], we estimate that the pressure of the energetic ions within the foreshock with energies between 30 and 300 keV increases by a factor of 2.5 from 1.5 to 5 min following the first contact of the IMF lines with the bow shock. Although the spectra soften, the pressure still increases due to the rapid increase in the energetic ion flux at the lowest energies. Rather than exploding and imploding, the cavity should grow steadily throughout the first 5 min of its existence.

[24] Past studies have attributed the regions of enhanced densities and magnetic field strengths bounding HFAs to fast mode shocks standing in the solar wind flow [e.g., *Schwartz et al.*, 1985; *Fuselier et al.*, 1987]. If the regions bounding our events contain shocked plasmas, then the shocks are very weak indeed. Whereas the ratios for shocked to ambient densities, velocities, ion temperatures, and magnetic field strengths were 3.5, 0.8, 3.3, and 3 for the event studied by *Fuselier et al.* [1987], they were only 1.2, 0.97, 1.17, and 1.2 for the first of the two events presented here, and even nearer 1.0 for the second event. Because the events reported in this paper move antisunward at speeds only slightly less than those of the solar wind flow, there is no need to invoke shocks. Instead, our events are probably bounded by fast mode waves.

[25] Whether the enhancements seen in our examples result from fast mode waves or shocks, we can determine their orientation from the required coplanarity of the magnetic field observations. Using the IMF observations at 2010:29 and 2011:57 UT, we find that the normal to the leading edge points in the GSE (x, y, z) = (−0.13, −0.45, 0.89) direction. Using the IMF observations at 2016:16 and 2020:35 UT, we find that the normal to the trailing edge points in the GSE (x, y, z) = (0.96, −0.02, 0.30) direction. Similar discrepancies between the normals on leading edges pointing transverse to the Sun-Earth line and normals on trailing edges pointing sunward have already been noted in past studies of HFAs and foreshock cavities [e. g., *Schwartz et al.*, 1988; *Sibeck et al.*, 2001].

[26] Finally, consider the IMF orientations favoring event detection. To be observed, the plasma and magnetic field perturbations observed within the events must attain finite amplitudes and extend finite distances away from the bow shock. On the dayside, these conditions are best met during periods of near-radial IMF orientation, when IMF lines sweep slowly across a nearly quasi-parallel bow shock. While the events may also occur during periods when the IMF lies nearly transverse to the Sun-Earth line, they may not reach either observable dimensions or amplitudes during the ~4 min required for a ~400 km s^{-1} solar wind flow to sweep them out of the region upstream from the dayside bow shock.

5. Conclusion

[27] Some characteristics of the foreshock cavities presented in this paper resemble those of HFAs. Like HFAs, foreshock cavities exhibit durations of 1–2 min, reduced densities and magnetic field strengths flanked by enhancements, and enhanced ion temperatures that increase gradually from the solar wind towards the core region of the events. However, many characteristics of the foreshock cavities differ from those of HFAs. There is no great reduction or deflection of flow velocities within the events, the ion populations never become nearly isotropic, ion temperatures never reach the values previously reported for HFAs, and pressures within the cavities are only slightly greater than those outside.

[28] The characteristics of foreshock cavities are consistent with the predictions of the *Thomas and Brecht* [1988] model for the interaction of a beam of backstreaming ions with the oncoming solar wind. We argued that distribution functions observed within the cavity were similar to those previously reported in the foreshock and attributed to Fermi acceleration. An explanation in terms of HFAs is neither needed nor available to us: we do not require the intense ion heating observed within HFAs or the peculiar particle acceleration at the sharp IMF discontinuities intersecting the bow shock that have been invoked to explain them.

[29] Others have reported events with characteristics similar to those presented here, but not offered a detailed explanation of their origin or a comprehensive comparison of their characteristics with the predictions of the model proposed by *Thomas and Brecht* [1988]. None of the foreshock events reported by *Wibberenz et al.* [1985], *Sibeck et al.* [1989], *Fairfield et al.* [1990], or *Sibeck et al.* [2001] lay centered upon an IMF discontinuity interacting with the bow shock. *Fairfield et al.* [1990] and *Sibeck et al.* [2001] reported that flow deflections were generally insignificant throughout the foreshock and in particular during observations of cavities. Ion temperatures within the events reported by *Sibeck et al.* [1989], *Fairfield et al.* [1990], and *Sibeck et al.* [2001] never exceeded 2×10^6 K. Consequently, we interpret all these events as the foreshock craters predicted by the *Thomas and Brecht* [1988] model rather than as HFAs predicted by the *Thomas et al.* [1991] model. By contrast to the handful of HFAs reported in the literature, *Sibeck et al.* [2001] identified 292 foreshock cavities in IMP-8 observations during a 7-month period during 1995. Apparently, foreshock cavities are far more common than HFAs.

[30] The significance of the foreshock cavities (and HFAs) lies in the role they play in modulating the solar wind-magnetosphere interaction. According to *Thomas et al.* [1995], pressure variations generated within the foreshock are simply transmitted downstream across the bow shock into the magnetosheath. Foreshock cavities provide a constantly changing pattern of pressures that can drive magnetopause motion and trigger reconnection on that

boundary. Understanding when and where foreshock cavities occur, as well as the amplitudes that they attain, should be an important objective of solar wind-magnetosphere interaction studies.

[31] **Acknowledgments.** The authors would like to thank both referees for helpful comments. Work at APL was supported in part by the NSF's ATM Space Weather Grant 9819707 and NASA's ISTP program grant NAG5-7920. Work at UC Berkeley was funded in part by NASA grant FDNAG5-6928.

[32] Hiroshi Matsumoto and Lou-Chuang Lee thank M. Hoshino and Bruce E. Goldstein for their assistance in evaluating this paper.

References

Anderson, K. A., R. P. Lin, F. Martel, C. S. Lin, G. K. Parks, and H. Réme, Thin sheets of energetic electrons upstream from the Earth's bow shock, *Geophys. Res. Lett.*, *6*, 401–404, 1979.

Fairfield, D. H., Average and unusual locations of the Earth's magnetopause and bow shock, *J. Geophys. Res.*, *76*, 6700–6716, 1971.

Fairfield, D. H., W. Baumjohann, G. Paschmann, H. Lühr, and D. G. Sibeck, Upstream pressure variations associated with the bow shock and their effects on the magnetosphere, *J. Geophys. Res.*, *95*, 3773–3786, 1990.

Fuselier, S. A., M. F. Thomsen, J. T. Gosling, S. J. Bame, C. T. Russell, and M. M. Mellott, Fast shocks at the edges of hot diamagnetic cavities upstream from the Earth's bow shock, *J. Geophys. Res.*, *92*, 3187–3194, 1987.

Gary, S. P., J. T. Gosling, and D. W. Forslund, The electromagnetic ion beam instability upstream of the Earth's bow shock, *J. Geophys. Res.*, *86*, 6691–6696, 1981.

Lepping, R. P., et al., The Wind magnetic field investigation, *Space Sci. Rev.*, *71*, 207–229, 1995.

Lin, Y., Generation of anomalous flows near the bow shock by its interaction with interplanetary discontinuities, *J. Geophys. Res.*, *102*, 24,265–24,282, 1997.

Lin, R. P., et al., A three-dimensional plasma and energetic particle investigation for the Wind spacecraft, *Space Sci. Rev.*, *71*, 125–153, 1995.

Mitchell, D. G., and E. C. Roelof, Dependence of 50-keV upstream ion events at IMP 7&8 upon magnetic field bow shock geometry, *J. Geophys. Res.*, *88*, 5623–5634, 1983.

Onsager, T. G., M. F. Thomsen, J. G. Gosling, and S. J. Bame, Observational test of a hot flow anomaly formation mechanism, *J. Geophys. Res.*, *95*, 11,967–11,974, 1990.

Paschmann, G., N. Sckopke, I. Papamastorakis, J. R. Asbridge, S. J. Bame, and J. T. Gosling, Characteristics of reflected and diffuse ions upstream from the Earth's bow shock, *J. Geophys. Res.*, *86*, 4355–4364, 1981.

Paschmann, G., G. Haerendel, N. Sckopke, E. Möbius, H. Lühr, and C.W. Carlson, 3-Dimensional plasma structures with anomalous flow directions near the Earth's bow shock, *J. Geophys. Res.*, *93*, 11,279–11,294, 1988.

Scholer, M., D. Hovestadt, F. M. Ipavich, and G. Gloeckler, Upstream energetic ions and electrons- Bow shock-associated or magnetospheric origin, *J. Geophys. Res.*, *86*, 9040–9046, 1981.

Schwartz, S. J., et al., An active current sheet sheet in the solar wind, *Nature*, *318*, 269–271, 1985.

Schwartz, S. J., R. L. Kessel, C. C. Brown, L. J. C. Woolliscroft, M. W. Dunlop, C. J. Farrugia, and D. S. Hall, Active current sheets near the Earth's bow shock, *J. Geophys. Res.*, *93*, 11,295–11,310, 1988.

Schwartz, S. J., G. Paschmann, N. Sckopke, T. M. Bauer, M. Dunlop, A. N. Fazarkerley, and M. F. Thomsen, Conditions for the formation of hot flow anomalies at Earth's bow shock, *J. Geophys. Res.*, *105*, 12,639–12,650, 2000.

Sibeck, D. G., et al., The magnetospheric response to 8-minute-period strong-amplitude upstream pressure variations, *J. Geophys. Res.*, *94*, 2505–2519, 1989.

Sibeck, D. G., R. B. Decker, D. G. Mitchell, A. J. Lazarus, R. P. Lepping, and A. Szabo, Solar wind preconditioning in the flank foreshock: IMP-8 observations, *J. Geophys. Res.*, *106*, 21,675–21,688, 2001.

Skadron, G., R. D. Holdaway, and M. Scholer, Perturbation of the solar wind in a model terrestrial foreshock, *J. Geophys. Res.*, *91*, 8798–8804, 1986.

Terasawa, T., Origin of 30∼100 keV protons observed in the upstream region of the Earth's bow shock, *Planet. Space Sci.*, *27*, 365 –384, 1979.

Thomas, V. A., and S. H. Brecht, Evolution of diamagnetic cavities in the solar wind, *J. Geophys. Res.*, *93*, 11,341–11,353, 1988.

Thomas, V. A., D. Winske, M. F. Thomsen, and T. G. Onsager, Hybrid simulation of the formation of a hot flow anomaly, *J. Geophys. Res.*, *96*, 11,625–11,632, 1991.

Thomas, V. A., D. Winske, and M. F. Thomsen, Simulation of upstream pressure pulse propagation through the bow shock, *J. Geophys. Res.*, *100*, 23,481–23,488, 1995.

Thomsen, M. F., J. T. Gosling, S. A. Fuselier, S. J. Bame, and C. T. Russell, Hot diamagnetic cavities upstream from the Earth's bow shock, *J. Geophys. Res.*, *91*, 2961–2973, 1986.

Thomsen, M. F., J. T. Gosling, S. J. Bame, K. B. Quest, C. T. Russell, and S. A. Fuselier, On the origin of hot diamagnetic cavities near the Earth's bow shock, *J. Geophys. Res.*, *93*, 11,311–11,325, 1988.

Wibberenz, G., F. Zöllich, H. M. Fischer, and E. Keppler, Dynamics of intense upstream ion events, *J. Geophys. Res.*, *90*, 283–301, 1985.

R. P. Lepping, D. G. Sibeck, and A. Szabo, Code 696, Goddard Space Flight Center, Greenbelt, MD 20771, USA. (david.sibeck@gsfc.nasa.gov)

R. Lin and T.-D. Phan, Space Sciences Laboratory, University of California, Centennial Dr. at Grizzly Peak Blvd., Berkeley, CA 94720-7450, USA.

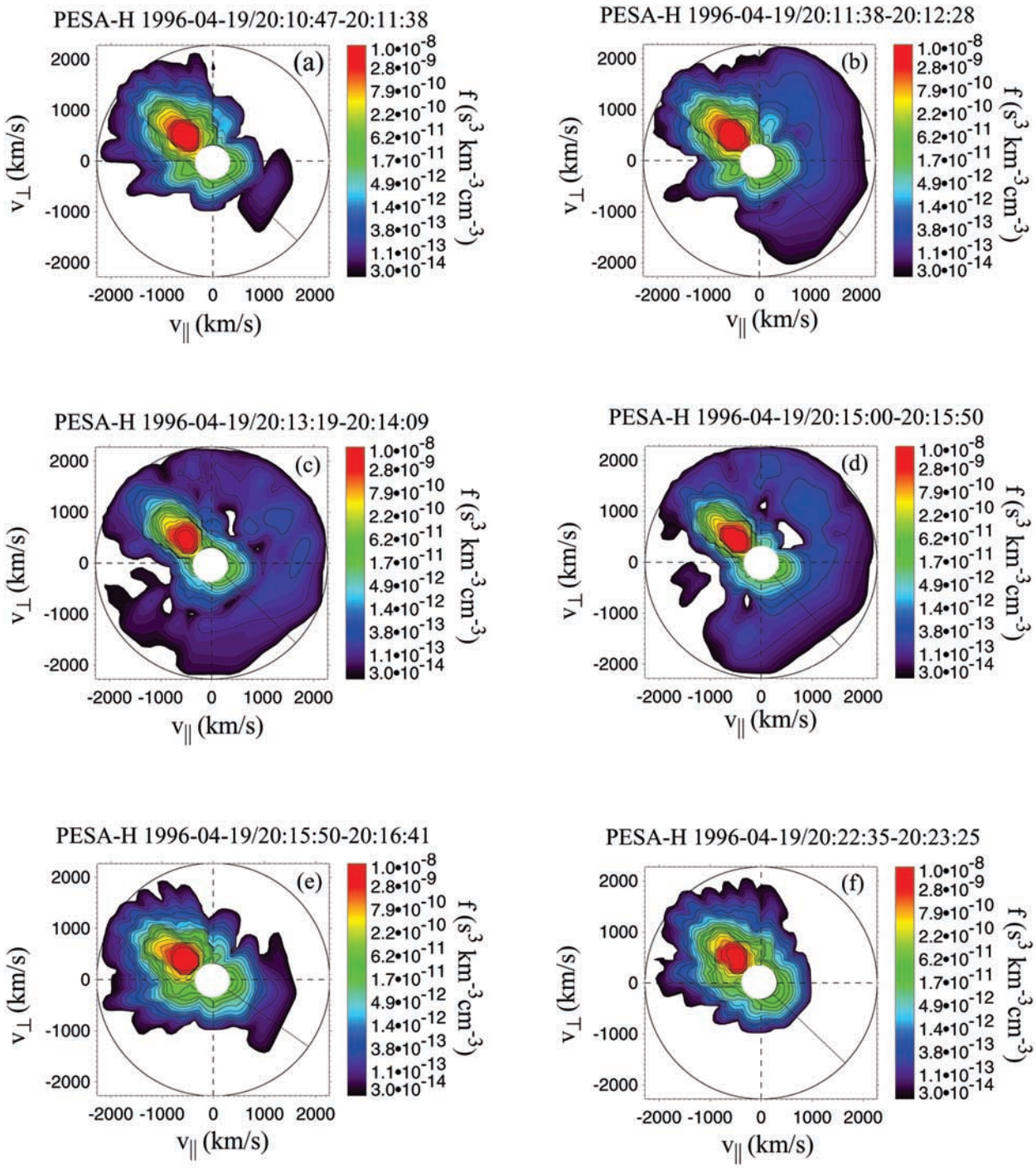

Figure 7. Wind 3DP PESA-H ion distribution functions from (a) 2010:47 to 2011:38, (b) 2011:38 to 2012:28, (c) 2013:19 to 2014:09, (d) 2015:00 to 2015:50, (e) 2015:50 to 2016:41, and (f) 2022:35 to 2023:25 UT.